

# Characterizing the multi-scale spatial structure of remotely sensed evapotranspiration with information theory

N. A. Brunsell<sup>1</sup> and M. C. Anderson<sup>2</sup>

<sup>1</sup>Dept. of Geography, University of Kansas, Lawrence, KS, USA

<sup>2</sup>Hydrology and Remote Sensing Lab, USDA, Beltsville, MD, USA

Received: 27 March 2011 – Published in Biogeosciences Discuss.: 30 March 2011

Revised: 14 July 2011 – Accepted: 17 August 2011 – Published: 22 August 2011

**Abstract.** A more thorough understanding of the multi-scale spatial structure of land surface heterogeneity will enhance understanding of the relationships and feedbacks between land surface conditions, mass and energy exchanges between the surface and the atmosphere, and regional meteorological and climatological conditions. The objectives of this study were to (1) quantify which spatial scales are dominant in determining the evapotranspiration flux between the surface and the atmosphere and (2) to quantify how different spatial scales of atmospheric and surface processes interact for different stages of the phenological cycle. We used the ALEXI/DisALEXI model for three days (DOY 181, 229 and 245) in 2002 over the Ft. Peck Ameriflux site to estimate the latent heat flux from Landsat, MODIS and GOES satellites. We then applied a multiresolution information theory methodology to quantify these interactions across different spatial scales and compared the dynamics across the different sensors and different periods. We note several important results: (1) spatial scaling characteristics vary with day, but are usually consistent for a given sensor, but (2) different sensors give different scalings, and (3) the different sensors exhibit different scaling relationships with driving variables such as fractional vegetation and near surface soil moisture. In addition, we note that while the dominant length scale of the vegetation index remains relatively constant across the dates, the contribution of the vegetation index to the derived latent heat flux varies with time. We also note that length scales determined from MODIS are consistently larger than those determined from Landsat, even at scales that should be detectable by MODIS. This may imply an inability of the MODIS sensor to accurately determine the fine scale spa-

tial structure of the land surface. These results aid in identifying the dominant cross-scale nature of local to regional biosphere-atmosphere interactions.

## 1 Introduction

Scaling issues are ubiquitous in land-atmosphere interactions (Brunsell and Gillies, 2003a; Anderson et al., 2003). They impact our ability to accurately model and measure the exchange of mass and energy across the surface atmosphere interface. Issues with scaling across different spatial and temporal resolutions is complicated through non-linear interactions (Raupach and Finnigan, 1995), feedbacks developing at preferential scales (Koster et al., 2004) as well as incorporating the impacts of spatial pattern on mass transfer (Schymanski et al., 2010). These issues may ultimately be impacting our ability to adequately address the impacts of global climate change (Wagener et al., 2010).

One aspect of the scaling problem involves aggregation of fine resolution data to accurately determine the areal average. This is complicated by the non-linearity of the exchange processes governing mass and energy transport (Raupach and Finnigan, 1995; Western et al., 2002). For example, the areal average value of evapotranspiration is not a function of the spatially averaged input fields such as air temperature. This is particularly problematic when attempting to estimate the fluxes from satellite data sources, as these platforms observe the spatially aggregated value of fields such as radiometric temperature at the satellite resolution.

An approach to confronting this aspect of the scaling problem is the “effective parameters” approach, in which the conceptual model (e.g. that the flux is proportional to the local scalar gradient) was deemed correct, and only the “true”



Correspondence to: N. A. Brunsell  
(brunsell@ku.edu)

value of a conductivity term had to be determined (Lhomme et al., 1994; Chehbouni et al., 2000). On a more theoretical level, this necessitates the assumption that the model physics are also applicable across the range of scales under consideration. Similar issues arise when downscaling from coarser to finer resolutions, where the problem involves accurately determining the distribution of the data at resolutions below that observed by the satellite (i.e. subgrid heterogeneity).

The use of satellite data provides the opportunity to achieve measurements at a variety of spatial resolutions, but the interpretation and validation of these measurements are often unclear (e.g. Wu and Li, 2009). When considering energy and mass fluxes derived from satellite data, it is necessary to employ some model that translates the input fields into the flux of interest. For example using a vegetation index and land surface temperature to derive the evaporative flux (e.g. Carlson, 2007). This application of a model also entails a scaling problem. A model calibrated to a particular resolution may or may not be useful when faced with a change of resolution, i.e. the so-called equifinality concept (Beven and Freer, 2001). McCabe et al. (2005) directly incorporated this concept into a land surface model for determining deriving temporal variability of evapotranspiration from remote sensing.

However, the application of a model across different spatial resolutions may also lead to different observed scaling relationships between modeled output fluxes and controlling variables (Brunsell and Gillies, 2003b). An additional problematic area that has not been given sufficient acknowledgement is when the models are developed using the preferred conceptual scales of different scientific disciplines (e.g. atmospheric scientists and ecophysicologists) result in perhaps contrary views of the underlying process (e.g. Jarvis and McNaughton, 1986).

It is generally felt that higher spatial resolution is better for accurately quantifying exchange processes between the land surface and the atmosphere. However, as the community moves to higher temporal and spatial resolution for global monitoring, there is a necessary increase in computational workload. In some cases higher resolution data may not be necessary, meaning that it may not contribute additional information about the process (e.g. Brunsell et al., 2008). For example, McCabe and Wood (2006) found that while MODIS was unable to ascertain the field scale evapotranspiration, it was able to accurately determine the watershed scale flux. However, a quantifiable method to determine this is necessary. Therefore, we are faced with the question: how can we assess the relative importance of different spatial scales of remotely sensed observations, particularly with respect to seasonal and interannual variations in phenology, soil moisture etc. on the spatial structure of modeled fluxes?

Recently, tools from information theory have been used to attempt to address this type of question. Stoy et al. (2009) attempted to ascertain the “optimum” pixel scale. Using Shannon entropy and the relative entropy (also called the

Kullback–Leibler divergence), they were able to calculate the amount of information contributed as the scale of observation was aggregated. Thus, they were able to define an “optimum” pixel resolution based on the loss of information.

In addition to assessing the role of pixel aggregation, information theory has also been used to examine the flow of information across the surface–atmosphere interface. Brunsell (2010) used the information theory metrics of entropy, mutual information content and relative entropy to assess spatial variation in the temporal scaling of daily precipitation. This technique was able to determine clear scale breaks in the temporal patterns of precipitation that were not captured by traditional techniques.

Brunsell and Young (2008) used the metrics to assess the information gained by surface vegetation as a function of the time scales of input precipitation field across the Missouri Basin using MODIS and NEXRAD data. They found a clear relationship between the information content and the resolution of the data. Brunsell et al. (2008) examined how evapotranspiration derived from satellite data was sensitive to different spatial scales of vegetation and soil moisture dynamics and found a clear sensitivity to topographic position and moisture content. Similarly, Ruddell and Kumar (2009) examined surface–atmosphere fluxes by quantifying the information transfer using eddy covariance observations. They were able to quantitatively define surface–atmosphere feedbacks using this technique.

The previous research has focused on assessing the information content and transfer using data from the same spatial or temporal resolutions. We are interested in continuing this line of research into the applicability of information theory metrics for assessing biosphere–atmosphere interactions. Here, we wish to examine how different initial spatial resolutions of satellite data impact the relationship between evapotranspiration and controlling variables such as soil moisture and vegetation cover as a function of spatial resolution. This is essential knowledge for understanding both our ability to observe scaling relationships as well as to model the impacts correctly across a wide range of scales.

## 2 Model Description

The Atmosphere Land Exchange Inverse (ALEXI) surface energy balance model was specifically designed to minimize the need for ancillary meteorological data while maintaining a physically realistic representation of land–atmosphere exchange over a wide range in vegetation cover conditions (e.g. Anderson et al., 2004). It is one of few land–surface models designed explicitly to exploit the high temporal resolution afforded by geostationary satellites like GOES.

Surface energy balance models estimate evapotranspiration ( $ET$ ,  $W m^{-2}$ ) by partitioning the energy available at the land surface ( $R_n - G$ ), where  $R_n$  is net radiation and  $G$  is the

soil heat conduction flux, in  $\text{W m}^{-2}$  into turbulent fluxes of sensible heat ( $H$ ,  $\text{W m}^{-2}$ ) and  $ET$ :

$$Rn - G = H + ET \quad (1)$$

Surface temperature is a valuable metric for constraining  $ET$  because varying soil moisture conditions yield a distinctive thermal signature: moisture deficiencies in the root zone lead to vegetation stress and elevated canopy temperatures, while depletion of water from the soil surface layer causes the soil component of the scene to heat up rapidly.

The land-surface representation in ALEXI model is based on the series version of the two-source energy balance (TSEB) model of Norman et al. (1995), which partitions the composite surface radiometric temperature,  $T_{\text{rad}}$ , into characteristic soil (denoted by the subscript S) and canopy (subscript C) temperatures,  $T_S$  and  $T_C$ , based on the local vegetation cover fraction ( $Fr$ ) apparent at the thermal sensor view angle,  $f(\theta)$ :

$$T_{\text{rad}}(\theta) \approx f(\theta)T_C + [1 - f(\theta)]T_S \quad (2)$$

For a homogeneous canopy with spherical leaf angle distribution and leaf area index (LAI),  $f(\theta)$  can be approximated as:

$$f(\theta) = 1 - \exp\left(\frac{-0.5 \text{ LAI}}{\cos\theta}\right) \quad (3)$$

With information about  $T_{\text{rad}}$ , LAI, and radiative and meteorological forcing, the TSEB evaluates the soil and the canopy energy budgets separately, computing system and component fluxes of net radiation ( $Rn = Rn_C + Rn_S$ ), sensible and latent heat ( $H = H_C + H_S$  and  $ET = ET_C + E_S$ ), and soil heat conduction ( $G$ ). Importantly, because angular effects are incorporated into the decomposition of  $T_{\text{rad}}$ , the TSEB can accommodate thermal data acquired at off-nadir viewing angles and can therefore be applied to geostationary satellite images.

The TSEB has a built-in mechanism for detecting thermal signatures of vegetation stress. A modified Priestley-Taylor relationship, applied to the divergence of net radiation within the canopy ( $Rn_C$ ), provides an initial estimate of canopy transpiration ( $ET_C$ ), while the soil evaporation rate ( $E_S$ ) is computed as a residual to the system energy budget. If the vegetation is stressed and transpiring at significantly less than the potential rate, the Priestley-Taylor equation will overestimate  $ET_C$  and the residual  $E_S$  will become negative. Condensation onto the soil is unlikely midday on clear days, and therefore  $E_S < 0$  is considered a signature of system stress. Under such circumstances, the Priestley-Taylor coefficient is throttled back until  $E_S \approx 0$  (expected under dry conditions). Both  $ET_C$  and  $E_S$  will then be some fraction ( $ET/PET$ ) of the potential  $ET$  rates associated with the canopy and soil.

For regional-scale applications, the TSEB has been coupled with an atmospheric boundary layer (ABL) model to internally simulate land-atmosphere feedback on near-surface

air temperature. In the ALEXI model, the TSEB is applied at two times during the morning ABL growth phase (approximately  $t_1 = 1.5$  and  $t_2 = 5.5$  h after local sunrise), using radiometric temperature data obtained from a geostationary platform like GOES at spatial resolutions of 5–10 km. Energy closure over this interval is provided by a simple slab model of ABL development (McNaughton and Spriggs, 1986), which relates the rise in air temperature in the mixed layer to the time-integrated influx of sensible heat from the land surface. As a result of this configuration, ALEXI uses only time-differential temperature signals, thereby minimizing flux errors due to absolute sensor calibration and atmospheric and spatial effects (Kustas et al., 2001). The primary radiometric signal is the morning surface temperature rise, while the ABL model component uses only the general slope (lapse rate) of the atmospheric temperature profile (Anderson et al., 1997), which is more reliably analyzed from synoptic radiosonde data than is the absolute temperature reference. To map fluxes at higher resolution than afforded by geostationary satellites (typically 5–10 km) a flux disaggregation technique referred to as DisALEXI (Norman et al., 2003) can be applied. DisALEXI is a nested modeling approach that uses air temperature diagnosed by ALEXI along with high resolution LAI and  $T_{\text{rad}}$  information from polar orbiting instruments like Landsat or MODIS or aircraft, normalized to conserve  $H$  at the GOES pixel scale. For comparison with tower fluxes, DisALEXI fluxes are reaggregated over the surface source area contributing to the sensor measurement, typically on the order of 100-m in dimension. Anderson et al. (2007) summarize ALEXI validation experiments yielding typical root-mean-square-deviations in comparison with tower flux measurements (30-min averages) of  $H$  and  $ET$  are 35–40  $\text{W m}^{-2}$  (15 % of the mean observed flux) over a range in vegetation cover types and climatic conditions. Further details about the ALEXI/DisALEXI modeling system are provided by Anderson et al. (2007).

### 3 Site description

The study area focuses on AmeriFlux tower site located outside of Fort Peck ( $48^\circ 18' 36''$ ,  $105^\circ 06' 00''$ , elevation = 634 m a.s.l.) in the northeast corner of Montana. The tower itself is situated in a grazed grassland along the Poplar River, but the Landsat scene also contains a significant fraction of rainfed and irrigated agricultural fields. The topography is predominantly flat, and there are several lakes and reservoirs contained within the scene. Soils around the site are moderately drained clay loams. See Wilson and Meyers (2007) for further details on the Fort Peck AmeriFlux site.

The remotely sensed imagery covers a domain of 102.4 km by 102.4 km centered on the tower location. We applied the ALEXI/DisALEXI models to derive evapotranspiration on three days: 30 June (DOY 181), 17 August (DOY 229), and 2 September (DOY 245) in 2002 over the AmeriFlux sites in Ft.

Peck Montana, USA. The Landsat imagery has a resolution of 100 m, while the MODIS and GOES imagery are resampled to match the 100 m resolution which is output from the ALEXI/DisALEXI models. These three days were chosen due to the relatively cloud free nature of the Landsat scenes on those dates. Rainfall was recorded at the tower in day prior to each day of analysis. However only DOY 228 received a large (18 mm) amount. The other days received 1.6 mm (DOY 181) and 0.6 mm (DOY 245).

## 4 Methods

### 4.1 Wavelets

We conducted a wavelet multiresolution analysis to examine the contribution of different spatial scales to the modeled *ET*. The wavelet transform is conducted via the translation and dilation of a mother wavelet  $\psi$  across a data set  $f$  as a function of time  $t$ :

$$W(m, n) = \lambda_0^{-m/2} \int_{-\infty}^{\infty} f(t) \psi(\lambda_0^{-m} t - nt_0) dt \quad (4)$$

where  $W$  are the wavelet coefficients,  $m$  is the dilation and  $n$  is the translation,  $\lambda_0$  is the initial scale and  $t_0$  is the initial translation. The initial scale is twice the resolution of the measurements and the initial translation is zero. In practice, the integration would be conducted over the full domain of interest and not to infinity. The wavelet is given by:

$$\psi_{m,n}(t) = \frac{1}{\sqrt{\lambda_0^m}} \psi\left(\frac{t - nt_0 \lambda_0^m}{\lambda_0^m}\right) \quad (5)$$

The two-dimensional wavelet analysis is conducted as three one-dimensional wavelet transforms (Kumar and Foufoula-Georgiou, 1993). These are conducted in the horizontal ( $\Psi^1(x, y)$ ), vertical ( $\Psi^2(x, y)$ ), and diagonal ( $\Psi^3(x, y)$ ) directions across the two dimensional dataset:

$$\Psi^1(x, y) = \phi(x) \psi(y) \quad (6)$$

$$\Psi^2(x, y) = \phi(y) \psi(x) \quad (7)$$

$$\Psi^3(x, y) = \psi(x) \psi(y) \quad (8)$$

where  $\phi$  is the scaling function corresponding to the mother wavelet.

The discrete detailed coefficients ( $Q_m$ ) at each scale are calculated by the inner product of the spatial data field  $f(x, y)$  and the wavelet transforms  $\Psi^i$ :

$$Q_m^{d1} f = \langle f, \Psi_{mnk}^1 \rangle \quad (9)$$

$$Q_m^{d2} f = \langle f, \Psi_{mnk}^2 \rangle \quad (10)$$

$$Q_m^{d3} f = \langle f, \Psi_{mnk}^3 \rangle \quad (11)$$

where the  $\langle \rangle$  denote the inner product.

This analysis returns band-pass filtered versions of the dataset at each scale of interest. Therefore, the original dataset ( $f(x, y)$ ) can be reconstructed from the coarsest scale (i.e. average) and the residual fluctuations ( $f'(x, y) = \sum Q_m^{d_i} f$ ) at each point  $(x, y)$ :

$$f(x, y) \approx \overline{f_m(x, y)} + \sum_{m \geq m_0} f'_m(x, y) \quad (12)$$

Band-pass and low-pass filtering was conducted for the information theory metrics. Information theory metrics from the band-pass filtered data were calculated using the detailed coefficients at each scale ( $Q_m$ ), while the low-pass filtered versions were calculated by progressively removing the finer scales in Eq. (12). This was done in order to ascertain both the relative contribution of each scale to the spatial variability (band-pass) as well as to investigate how the different resolutions of the input the data would appear when filtered to the coarser resolutions. These filtered reconstructions are then used to compute the information theoretic metrics at each spatial scale as described next.

### 4.2 Information theory metrics

In order to assess the statistical variability of the precipitation fields, we combine the wavelet multi-resolution analysis with the information theory metrics of entropy ( $I$ ) and the relative entropy ( $R$ ).

The Shannon entropy is calculated as:

$$I(x) = - \sum_{i=1}^n p(x_i) \log(p(x_i)) \quad (13)$$

where  $p(x_i)$  is the probability density function (pdf) of variable  $x$  within a discrete bin  $i$  of the probability density function. Entropy is a measure of the statistical uncertainty of the random field  $x$  as described by the pdf. The entropy is a measure of the information (more information results in lower entropy and vice versa).

In addition to the entropy, the relative entropy ( $R(x, y)$ ) was also calculated. This is a measure of the distance between the probability density functions of the two variables  $x$  and  $y$  given by  $p$  and  $q$  respectively. Here  $p$  represents the pdf of the evapotranspiration and  $q$  represents either a coarser scale approximation given from the wavelet decomposition to  $p$  or of the remotely sensed fields of  $T_{rad}$ ,  $Rn$ , and  $Fr$ . Then  $R(x, y)$  is calculated as:

$$R(x, y) = \sum_i p_i \log\left(\frac{p_i}{q_i}\right) \quad (14)$$

This can be interpreted as the amount of additional information necessary to represent  $p$  given  $q$ . Thus, the smaller the value, the better the agreement between  $q$  and  $p$ .

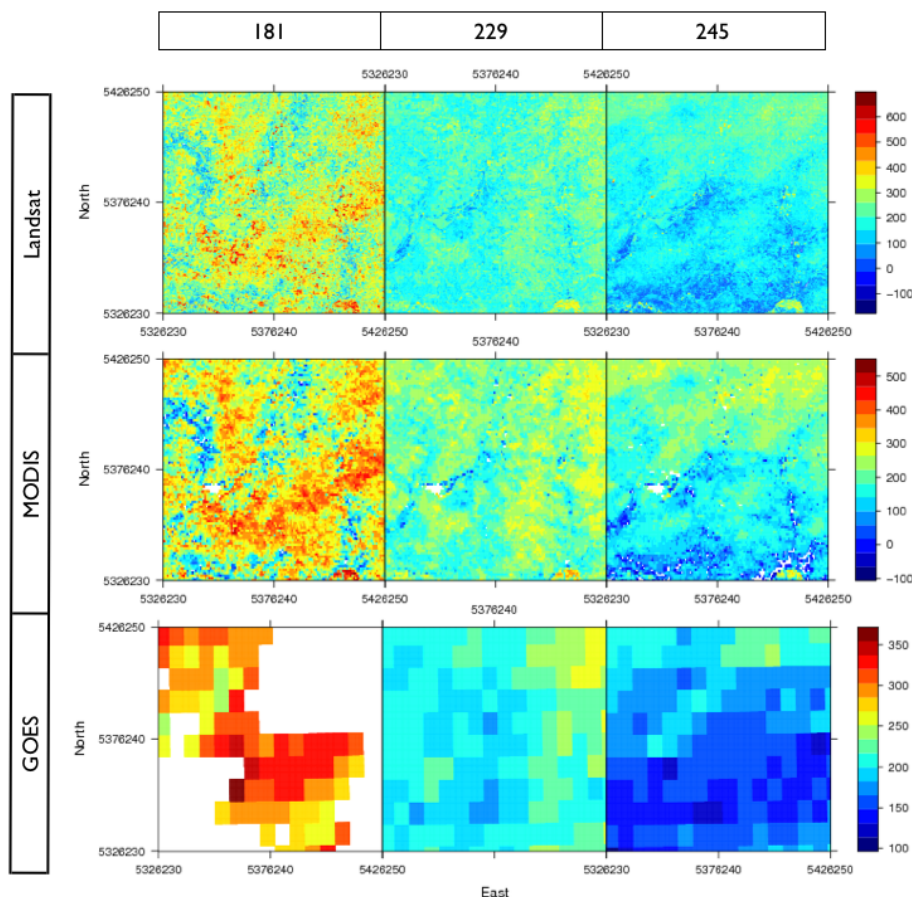


**Fig. 1.** ALEXI modeled  $ET$  fluxes [ $W m^{-2}$ ] over Ft. Peck Montana USA for three days (left) 181, (middle) 229 and (right) 245 in 2002 derived from three sensors (top) Landsat (middle) MODIS and (bottom) GOES.

## 5 Results

### 5.1 Spatial structure of remotely sensed fields and evapotranspiration

We applied the ALEXI/DisALEXI models to derive evapotranspiration on three days: 30 June (DOY 181), 17 August (DOY 229), and 2 September (DOY 245) in 2002 over the Ameriflux sites in Ft. Peck Montana, USA. The modeled  $ET$  fluxes for each of the days as derived from the sensors Landsat and MODIS (DisALEXI) and GOES (ALEXI) are shown in Fig. 1. Note that the range of modeled  $ET$  fluxes increases with the higher resolution satellites, as would be expected. On each day the observed spatial structure is generally captured by each of the satellites, but this structure does appear to change with time.

The mean  $ET$  flux and spatial standard deviation for each day derived from each sensor are shown in Table 1. In addition to the  $ET$  flux, we have also shown the mean and standard deviations for  $R_n$ ,  $T_{rad}$ ,  $Fr$ , and the ratio of actual to potential  $ET$  ( $ET/PET$ ) all evaluated under clear-sky conditions when  $T_{rad}$  can be retrieved from thermal band imagery.

Here,  $ET/PET$  is used as a proxy for soil moisture content, sampling the root-zone in well-vegetated areas and the soil surface layer (top 5 cm) in areas with sparse vegetation (Hain et al., 2011). Each sensor captures the same temporal trend in  $ET$ : maximum value on DOY 181 and decreasing with time. All of the sensors show approximately the same spatial mean as well, although the MODIS value on day 181 is slightly reduced compared to the other sensors. This same trend was observed in the  $R_n$  values, but not in the  $T_{rad}$ . The temperature values show a maximum on day 181, but a minimum on day 229, presumably due to a prior precipitation event. This is supported by the peak in the soil moisture proxy ( $ET/PET$ ) on this day observed by both the Landsat and MODIS sensors. The fractional vegetation shows the expected trend of a maximum value on day 181 and decreasing with time. Both the Landsat and MODIS sensors observe approximately the same values of fractional cover.

To determine the changes in the spatial structure of the  $ET$  flux we calculated the wavelet spectra from each sensor for each day (Fig. 2). The overall wavelet variance (area under the curve) is highest for day 181, while the other days show approximately the same curves for both the Landsat

**Table 1.** Spatial mean and standard deviation in parentheses for evapotranspiration ( $ET$ , [ $\text{W m}^{-2}$ ]), net radiation ( $Rn$ , [ $\text{W m}^{-2}$ ]), surface temperature ( $T_{\text{rad}}$ , [C]), fractional vegetation ( $Fr$ , [-]), and water limitation ( $ET/PET$ , [-]) for each sensor (Landsat, MODIS, and GOES) for each day of consideration (181, 229, and 245).

Sensor	Date	$ET$ [ $\text{W m}^{-2}$ ]	$Rn$ [ $\text{W m}^{-2}$ ]	$T_{\text{rad}}$ [C]	$Fr$ [-]	$ET/PET$ [-]
Landsat	181	301 (104)	636 (28)	30.9 (3.5)	0.53 (0.17)	0.66 (0.19)
	229	208 (53)	527 (18)	21.6 (2.5)	0.26 (0.12)	0.75 (0.16)
	245	166 (61)	478 (19)	26.8 (3.0)	0.22 (0.09)	0.60 (0.20)
MODIS	181	276 (87)	649 (17)	32.7 (2.2)	0.50 (0.09)	0.61 (0.17)
	229	215 (42)	549 (11)	22.2 (1.8)	0.27 (0.07)	0.74 (0.13)
	245	170 (59)	498 (14)	27.4 (2.5)	0.21 (0.06)	0.59 (0.19)
GOES	181	297 (26)	627 (8)	28.7 (0.8)	–	–
	229	210 (18)	523 (6)	20.6 (1.0)	–	–
	245	169 (25)	476 (7)	25.9 (1.3)	–	–

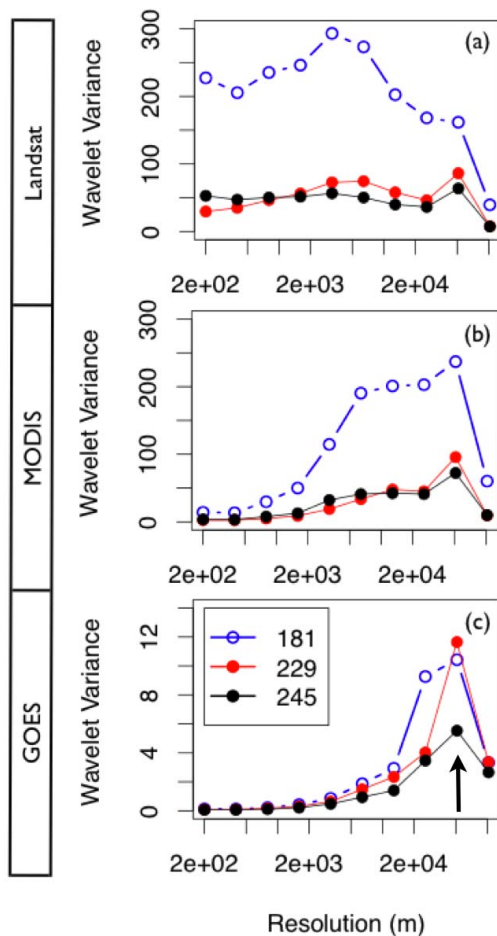


**Fig. 2.** Spatial wavelet spectra [Power  $\text{m}^{-1}$ ] for evapotranspiration for each sensor (Landsat, MODIS, and GOES) for each day of consideration (181, 229, and 245). The arrow denotes the 51 km scale.

and MODIS sensors. The Landsat data (panel a) shows a dominant length scale (peak of the wavelet spectra) on the order of 3.2 km for day 181, with large contributions from all but the largest scale (102 km). For dates 229 and 245, the role of this dominant scale is decreased and while the spectra is relatively flat, there does seem to be a peak in the range of 51 km.

The MODIS data (Fig. 2b) also shows larger spatial variance on day 181, but does not capture the 3.2 km length scale. The spectra is relatively constant over the range of 6 to 51 km, with a slight peak at the 51 km scale. This peak becomes slightly more pronounced on the later dates.

The GOES sensor (Fig. 2c) shows the same spatial structure regardless of the day of consideration, with a dominant length scale on the order of 51 km. The range of this length scale is slightly increased on day 181, exhibited by an increased contribution to the variance from a smaller spatial scale (25 km). As time progresses, the overall variance in the GOES signal decreases.

In addition to calculating the wavelet spectra for the  $EET$  flux, we also calculated the spectra for the dominant controlling variables of surface temperature, net radiation, and fractional vegetation (Fig. 3). The Landsat wavelet spectra for radiometric temperature (panel a) and net radiation (panel d) show the same general behavior, with substantially higher wavelet variance on DOY 181, and reduced values on the other days. Similar to the wavelet spectra for  $ET$ , we see an increase in the dominant length scale from the 3.2 km scale to the 51 km scale as time progresses, although the 3 to 6 km range continues to contribute significant portions of the overall variance. The  $Fr$  spectra (panel g) shows the same spatial structure on all days with a peak at the 3.2 km scale, and the overall variance decreases with time.

The MODIS spectra show the same general dominant length scale (51 km) regardless of the day of consideration for both the  $T_{\text{rad}}$  and  $Rn$  data fields (panels b and e). The

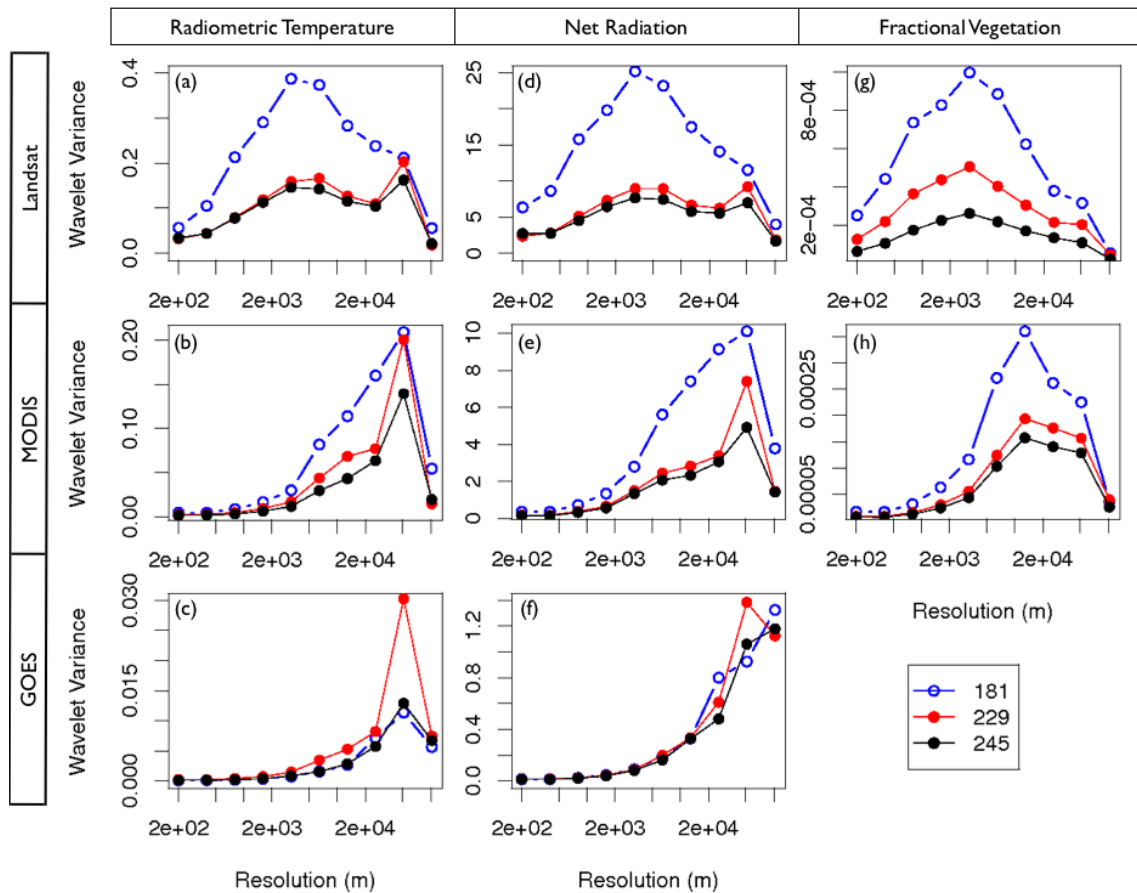


**Fig. 3.** Spatial wavelet spectra [ $\text{Power m}^{-1}$ ] for radiometric temperature, net radiation, and fractional vegetation for each sensor (Landsat, MODIS, and GOES) for each day of consideration (181, 229, and 245).

MODIS data also shows a general decrease in the overall wavelet variance as time progresses from DOY 181 to 229 to 245. The spectra show a reduced length scale for the fractional vegetation field relative to the temperature and net radiation, with a peak on the order of 6 km for each of the days.

The GOES data (panels c and f) generally shows the same structure and variance with a spike in the DOY 229 radiometric temperature data. The length scale for the GOES temperature data is the same as the MODIS length scale (51 km), while the  $Rn$  from GOES is continuously increasing across the range of scales considered here.

### 5.2 Multiresolution entropy of evapotranspiration

Next we applied the multiresolution information theory approach to quantify the information content of  $ET$  and associated data fields. An example of the approach is illustrated in Fig. 4, where we conducted a multiresolution analysis using a band-pass filter on the modeled  $ET$  derived from each of the sensors for day of year 181. Panel a shows the decomposed spatial fields for two selected scales (200 m and 51.2 km). The 200 m scale is below the resolution of the MODIS and GOES sensors, so not surprisingly, there is little variability at

this scale. The 51 km scale, on the other hand, is remarkably similar regardless of the sensor.

While the spatial structure in Fig. 4 looks similar, the spatial probability density functions do show some variability as a function of the initial sensor. At the 51 km scale, MODIS and GOES both show an increased number of pixels in the  $-20$  to  $20 \text{ W m}^{-2} ET$  range (recall that these are the values contributed from only this scale, not the total flux), while the Landsat observed more of a single peak. When considering the difference in the density functions between Landsat and MODIS, this may point to a fundamental difference in the ability of the two sensors to detect small changes in the structure of the spatial field.

From the probability density functions, we calculated the scalewise entropy (Fig. 5) using both band-pass and low-pass filtered versions of the  $ET$  flux for each sensor on each day. Since the band-pass filter decomposes the initial data field into only the contribution from an individual scale, the associated entropy represents the information content of the flux at that scale. Thus, this can be viewed as addressing “how much information is contributed from that scale to the total signal?” In the case of the Landsat  $ET$  flux (panel a), we see

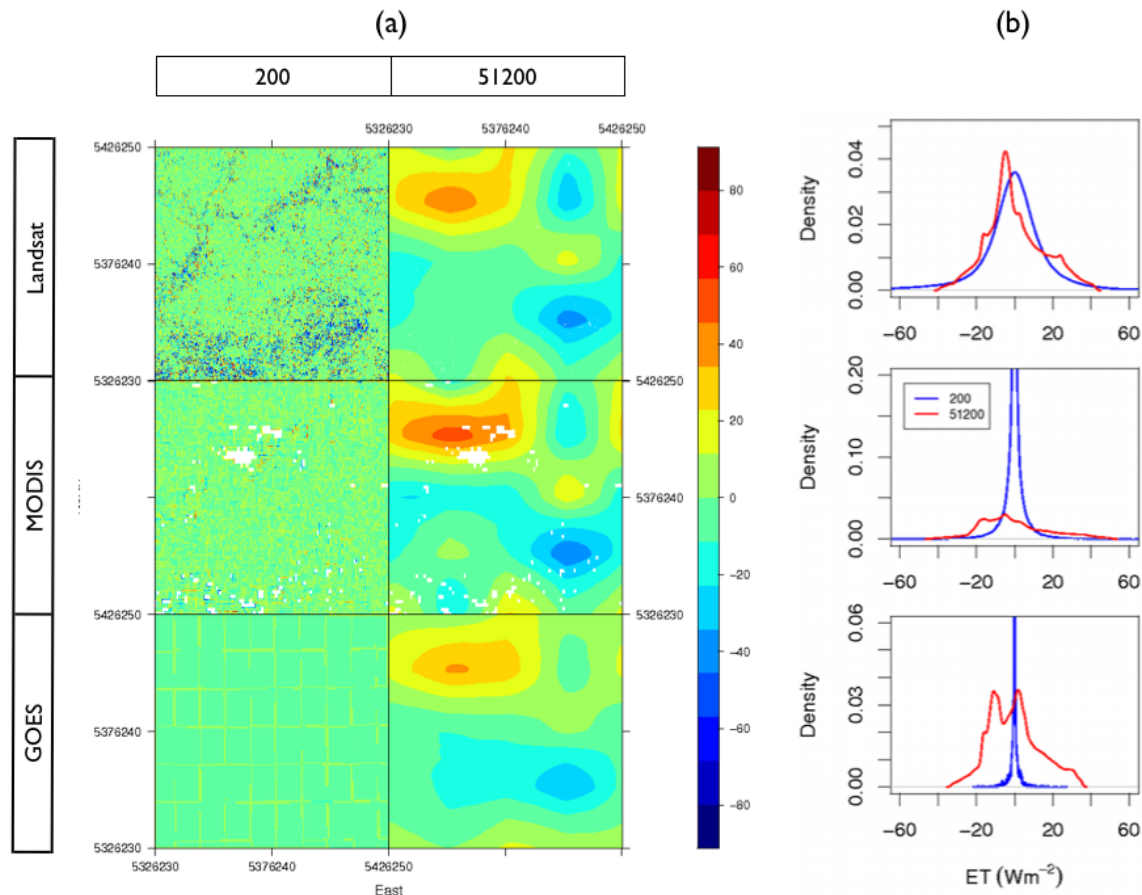


**Fig. 4.** (a) Example of band pass filtered evapotranspiration [ $\text{W m}^{-2}$ ] fields for day 181 for (top) Landsat (middle) MODIS and (bottom) GOES at two levels of decomposition (left) 200 m and (right) 51 200 m. Note that values indicate only the flux contributed from the individual scale, not the total evapotranspiration. (b) Shows the associated probability functions for each image in (a).

that each scale is contributing approximately equally to the observed information content. There is a slight reduction in the contribution from the largest scale on the later dates.

The MODIS data (panel b) shows a similar result, however with little information being contributed at the smallest scales due to the fact that these are below the resolution of the sensor. On days 229 and 245, there is slight peak in the information contributed at the 25 km scale. The GOES data shows a similar behavior across scales (panel c).

The low-pass filtered version of the data is helpful for addressing the question: “how much information is lost as we use coarser resolution data?” The Landsat data for day 181 (Fig. 5d), shows an almost continuous drop in information as the spatial resolution is coarsened. While for the other dates, this drop in information content is less significant until the larger spatial scales. The information content from MODIS *ET* (panel e), shows almost the same information content until scales on the order of 25 km. The GOES data is similar, with the exception of day 181, where there is actually increased information in the coarser scales.

### 5.3 Relative entropy between evapotranspiration and other fields

To further understand the nature of multiscale interactions responsible for determining the evapotranspiration flux, we made use of the relative entropy metric. We can examine how much information in the spatial structure of *ET* is due to the variability of other fields ( $T_{\text{rad}}$ ,  $R_n$ ,  $Fr$  etc.) as a function of spatial scale.

We calculated the relative entropy between the original scale *ET* and the band-pass filtered versions of the radiometric temperature and net radiation (Fig. 6). Recall that the higher values of RE indicate that more information is necessary to reconstruct the *ET* flux, thus the less information is being contributed by that scale to the evapotranspiration.

The relative entropy between the Landsat *ET* and  $T_{\text{rad}}$  is shown in Fig. 6a. The *RE* values show relatively constant variation across scale, with an increase in the RE at the smallest scales. In addition, this contribution becomes larger as time passes, thus indicating that the *ET* flux became less dependent upon small scale variations in surface temperature.

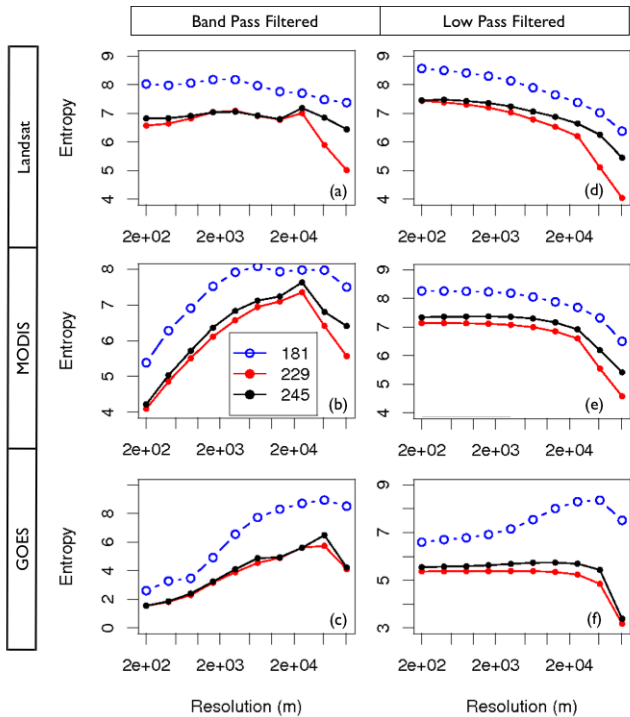


**Fig. 5.** Multiresolution entropy computed from low-pass (left) and band-pass (right) wavelet reconstructions for each sensor (rows) and each day (lines).

This is also observed in the MODIS data (panel b). In addition, the MODIS data exhibits an interesting variation across the smallest scales, where the scales up to 3.2 km become increasingly less important with time. The GOES sensor is generally unable to detect any change in the contribution as a function of time, except that day 181 actually shows higher *RE* values than the other dates contrary to what is observed in the other sensors.

The role of net radiation on the spatial structure of the evapotranspiration flux is also shown in Fig. 6. The *RE* between *R<sub>rad</sub>* and *ET* from Landsat (panel d) shows the same variation for days 181 and 229, with slightly higher values at the smallest scales. Day 245, however, shows a large increase at all scales, in particular the smallest scales up to the 3.2 km range (except 400 m). The relative entropy from MODIS (panel e), shows a different behavior, where days 229 and 245 show generally the same values and day 181 shows a similar relationship, but reduced values. The GOES data (panel f) shows the same behavior as the MODIS sensor.

Figure 7 shows the relative entropy between *ET* and the fractional vegetation and near surface water conditions. Again, recall that since the GOES sensor does not have a near-infrared band, these values are only computed for the Landsat and MODIS sensors. The fractional vegetation (panels a and b) show the same behavior as the radiometric temperature did for the respective sensor. Landsat exhibits a large increase in the *RE* on day 245, with increasing *RE* at

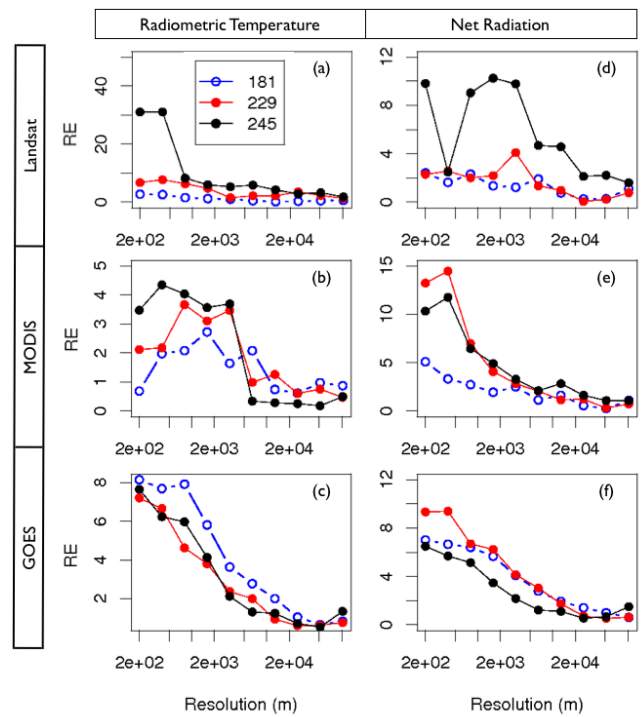


**Fig. 6.** Relative entropy between each scale of controlling variable (left)  $T_{rad}$  and (right)  $R_n$  to the modeled *ET* flux from each sensor for each day for (top) Landsat (middle) MODIS and (bottom) GOES for each day.

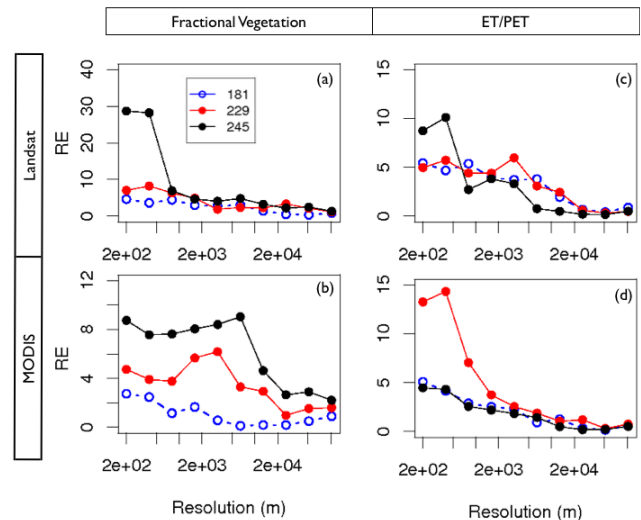


**Fig. 7.** Relative entropy between each scale of controlling variables (left) *F<sub>c</sub>* and (right) *ET/PET* to the modeled *ET* flux from each sensor for each day for (top) Landsat and (bottom) MODIS.

the smallest scales through time. The relative entropy from MODIS (panel b) shows a pronounced increase with time up to the 6.4 km scale.

The relative entropy between *ET* and *ET/PET* from Landsat (Fig. 7, panel c) shows generally the same behavior regardless of the day. As the spatial scale decreases, the *RE*

increases indicating more additional information is necessary to capture the true *ET* behavior. Larger RE values are seen at the smallest scale on day 245. MODIS RE values (panel d) show the same behavior on days 181 and 245, with day 229 exhibiting much larger values at the smallest scales. Since this date has the highest values of *ET/PET*, we expect that this is due to the combination of the resolution of MODIS and the convective nature of precipitation impacting the spatial scales of soil moisture. This is confirmed by the fact that the site received 18 mm of rainfall on day 228.

## 6 Discussion

The information content of a modeled field such as evapotranspiration is dependent upon both interactions between the processes determining the evaporative flux such as vegetation and soil moisture dynamics and the resolution of the initial data. Characterizing the nature of the relationship with the initial data resolution is a primary objective of this paper.

We have shown that the change in information content with resolution can be remarkably small (low pass filtered entropies shown in Fig. 5), and it may not be necessary to resort to the highest possible resolution of data to adequately characterize the spatial dynamics associated with the evaporative flux in a statistical sense. Obviously, however, the higher resolution data can provide information to the original data series (band pass filtered entropies in Fig. 5).

It is not particularly surprising that GOES is incapable of determining the finer spatial structure that Landsat and MODIS is capable of. However, it was somewhat surprising that Landsat fields decomposed to very coarse resolutions (e.g. compare DOY 245 in Fig. 5 panels d and f at the larger spatial scales) could still possess higher entropy values than finer resolution GOES data.

More significantly, the relationship between modeled flux and the input variables depends on the sensor. This is most clearly seen when examining the relative entropies between the controlling variables of  $T_{\text{rad}}$ ,  $R_n$ ,  $Fr$ , and *ET/PET* between Landsat and MODIS. Even at scales that both sensors can resolve, we have shown that different sensors exhibit different sensitivities to quantities such as the near surface moisture condition *ET/PET* or changes in the spatial structure of the vegetation as captured in the relationships with  $Fr$  (Fig. 7).

This could indicate that MODIS is incapable of capturing the small scale spatial structure as exhibited in the wavelet variance in Fig. 3. The length scales of variability determined from MODIS are consistently larger than those determined by Landsat even for scales that are detectable by the MODIS sensor. Note that this does not imply that MODIS and GOES are not capable of providing accurate estimation of the larger scale fluxes (McCabe and Wood, 2006).

Taken together these results suggest that the MODIS sensor is unable to fully characterize the fine spatial structure

of the land surface, and the different sensors characterize the interactions with fundamental variables (e.g. fractional vegetation and soil moisture) differently. This has large potential ramifications for the assessment of land surface interactions across spatial scales. It is essential to note that these changes in the observed interactions are not limited to the smallest scales (e.g. below the resolution of MODIS), these are at scales (e.g. 2–6 km) that MODIS should be able to detect (Fig. 7b and d).

Of course, it remains to be seen how general these results are. We have examined three dates over one relatively small geographic area. How land cover, vegetation phenology, etc. impact these results remains to be seen. However, there is clear evidence that changes in the spatial structure of soil moisture as determined from the wavelet spectra has a clear impact on the spatial structure of the evapotranspiration (e.g. DOY 229, Fig. 7d). In addition, the seasonal variation in the vegetation productivity as seen in the wavelet spectra also has a clear imprint on the evapotranspiration (Fig. 7b).

A related issue that is beyond the scope of the present work is the role of the higher temporal coverage provided by the MODIS and GOES sensors. There is the generally acknowledged trade off between spatial resolution and temporal coverage in remote sensing, but how this trade off actually impacts the information transfer should be investigated more deeply.

This raises an additional question for future research: how does the scale of observation impact our ability to model biosphere-atmosphere interactions at different spatial and temporal scales? First, however, we must be able to have some understanding of how these dynamics change across scale and what the potential ramifications may be. Only then can we possibly begin to incorporate such dynamics into the physically based models.

We are inherently assuming that the values derived from the higher resolution source (i.e. Landsat) are correct. There is no real evidence to support this assumption, and perhaps this is simply another aspect of the scale problem that the community is largely ignoring. Or perhaps, we are simply susceptible to the same inherent assumption that higher resolution data is fundamentally better. Maybe a better statement of this assumption is simply that different data sources provide fundamentally different information and we must use them all equally in order to fully characterize the cross-scale nature of biosphere-atmosphere interactions.

In order to address these types of concerns, models such as ALEXI which are inherently designed to make use of different resolution data simultaneously are necessary for examining these dynamics. These provide a necessary tool for quantifying the model sensitivity to changes in the initial spatial and/or temporal resolution of the input data.

## 7 Conclusions

We have applied a wavelet based multiresolution analysis combined with information theory metrics to assess the question: what is the relative importance of different spatial scales of the remotely sensed observations and the spatial structure of modeled fluxes? When considering the three dates used in this analysis, we can also begin to assess the impacts of seasonal variations in phenology, soil moisture etc. We have applied the ALEXI model to three days of data for which we have Landsat, MODIS and GOES data estimates of the evaporative flux.

There are several important results from this research, including (1) spatial scaling characteristics vary with day, but are usually (though not always) consistent for a given sensor, but (2) different sensors give different scalings. (3) Different sensors show different scaling relationships with the driving variables. This is related to cross-scale interactions between different controlling variables and the model *ET* as well as the inherent resolution of the initial data. We also note that while the dominant length scale of the vegetation index remains relatively constant across the dates, the contribution of the vegetation index to the derived latent heat flux changes with time. The length scales of variability are consistently larger when determined from MODIS data compared to Landsat, even when the Landsat derived length scales are at scales detectable by MODIS.

These results highlight the importance of explicitly accounting for spatial scaling when considering non-linear interactions that govern biosphere–atmosphere exchange processes. The proposed methodology is one such technique for determining such scaling dynamics. Additional research is necessary in order to understand the biophysical processes which give rise to the observed scaling characteristics.

*Acknowledgements.* We would like to thank one anonymous reviewer and Pete Falloon for their comments on a prior version of this paper. In addition, we would like to acknowledge the National Science Foundation grant number DEB-1021095 and subaward G214-11-W3336 for funding.

Edited by: M. Marconcini

## References

- Anderson, M. C., Norman, J., Diak, G., Kustas, W., and Mecikalski, J. R.: A two-source time-integrated model for estimating surface fluxes using thermal infrared remote sensing, *Remote Sens. Environ.*, 60(2), 195–216, 1997.
- Anderson, M. C., Kustas, W. P., and Norman, J. M.: Upscaling and downscaling – a regional view of the soil-plant-atmosphere continuum, *Agronom. J.*, 95, 1408–1423, 2003.
- Anderson, M. C., Norman, J., Mecikalski, J., Torn, R., Kustas, W., and Basara, J.: A multiscale remote sensing model for disaggregating regional fluxes to micrometeorological scales, *J. Hydrometeorol.*, 5, 343–363, 2004.
- Anderson, M. C., Norman, J., Mecikalski, J., Otkin, J., and Kustas, W.: A climatological study of evapotranspiration and moisture stress across the continental United States based on thermal remote sensing: 1. Model formulation, *J. Geophys. Res.*, 112, D10117, 1–17, 2007.
- Beven, K. and Freer, J.: Equifinality, data assimilation, and uncertainty estimation in mechanistic modelling of complex environmental systems using the GLUE methodology, *J. Hydrol.*, 249, 11–29, 2001.
- Brunsell, N. A.: A multiscale information theory approach to assess spatial–temporal variability of daily precipitation, *Journal of Hydrology*, 385, 165–172, doi:10.1016/j.jhydrol.2010.02.016, 2010.
- Brunsell, N. A. and Gillies, R.: Scale issues in land-atmosphere interactions: implications for remote sensing of the surface energy balance, *Agr. For. Meteorol.*, 117, 203–221, 2003a.
- Brunsell, N. A. and Gillies, R.: Length scale analysis of surface energy fluxes derived from remote sensing, *J. Hydrometeorol.*, 4, 1212–1219, 2003b.
- Brunsell, N. A. and Young, C. B.: Land surface response to precipitation events using MODIS and NEXRAD data, *Int. J. Remote Sens.*, 29, 1965–1982, doi:10.1080/01431160701373747, 2008.
- Brunsell, N., Ham, J., and Owensby, C.: Assessing the multi-resolution information content of remotely sensed variables and elevation for evapotranspiration in a tall-grass prairie environment, *Remote Sens. Environ.*, 112, 2977–2987, 2008.
- Carlson, T.: An overview of the “triangle method” for estimating surface evapotranspiration and soil moisture from satellite imagery, *Sensors*, 7, 1612–1629, 2007.
- Chehbouni, A., Watts, C., Kerr, Y., Dedieu, G., Rodriguez, J., Santiago, F., Cayrol, P., Boulet, G., and Goodrich, D.: Methods to aggregate turbulent fluxes over heterogeneous surfaces: application to SALSA data set in Mexico, *Agr. For. Meteorol.*, 105, 133–144, 2000.
- Hain, C., Crow, W., Mecikalski, J., Anderson, M. and Holmes, T.: An intercomparison of available soil moisture estimates from thermal-infrared and passive microwave remote sensing and land-surface modeling, *J. Geophys. Res.*, 116, D15107, 18 pp., doi:10.1029/2011JD015633, 2011.
- Jarvis, P. and McNaughton, K.: Stomatal control of transpiration: scaling up from leaf to region., *Adv. Ecol. Res.*, 15, 1–49, 1986.
- Koster, R., Dirmeyer, P., Guo, Z., Bonan, G., Chan, E., Cox, P., Gordon, C., Kanae, S., Kowalczyk, E., and Lawrence, D.: Regions of strong coupling between soil moisture and precipitation, *Science*, 305, 1138–1140, 2004.
- Kumar, P. and Foufoula-Georgiou, E.: A multicomponent decomposition of spatial rainfall fields. 1. Segregation of large- and small-scale features using wavelet transforms, *Water Resour. Res.*, 29, 2515–2532, 1993.
- Kustas, W., Diak, G., and Norman, J.: Time difference methods for monitoring regional scale heat fluxes with remote sensing, in *Land Surface Hydrology, Meteorology, and Climate: Observations and Modeling*, ed. Lakshmi, V., Albersson, J., and Schaake, J., *Am. Geophys. Union Water Sci. Appl. Ser.*, 3, 15–29, 2001.
- Lhomme, J. P., Chehbouni, A., and Monteny, B.: Effective parameters of surface energy balance in heterogeneous landscape, *Boundary Layer Meteorology*, 71, 297–309, 1994.
- McCabe, M. and Wood, E.: Scale influences on the remote estimation of evapotranspiration using multiple satellite sensors, *Re-*

- ote Sens. Environ., 105, 4, 271–285, 2006.
- McCabe, M., Kalma, J., and Franks, S.: Spatial and temporal patterns of land surface fluxes from remotely sensed surface temperatures within an uncertainty modelling framework, *Hydrol. Earth Syst. Sci.*, 9, 467–480, 2005, <http://www.hydrol-earth-syst-sci.net/9/467/2005/>.
- McNaughton, K. and Spriggs, T.: A mixed-layer model for regional evaporation, *Bound.-Lay. Meteorol.*, 36, 243–262, 1986.
- Norman, J., Kustas, W., and Humes, K.: Source approach for estimating soil and vegetation energy fluxes in observations of directional radiometric surface temperature, *Agr. For. Meteorol.*, 77, 263–293, 1995.
- Raupach, M. and Finnigan, J.: Scale issues in boundary-layer meteorology: surface energy balances in heterogeneous terrain, *Hydrol. Proc.*, 9, 589–612, 1995.
- Ruddell, B. L. and Kumar, P.: Ecohydrologic process networks: 1. Identification, *Water Resour. Res.*, 45, W03419, doi:10.1029/2008WR007279, 2009.
- Schymanski, S. J., Kleidon, A., Stieglitz, M., and Narula, J.: Maximum entropy production allows a simple representation of heterogeneity in semiarid ecosystems, *Phil. Trans. Roy. Soc. B: Biol. Sci.*, 365, 1449–1455, doi:10.1098/rstb.2009.0309, 2010.
- Stoy, P. C., Williams, M., Spadavecchia, L., Bell, R. A., Prieto-Blanco, A., Evans, J. G., and Wijk, M. T.: Using information theory to determine optimum pixel size and shape for ecological studies: Aggregating land surface characteristics in Arctic ecosystems, *Ecosystems*, 12, 574–589, doi:10.1007/s10021-009-9243-7, 2009.
- Wagener, T., Sivapalan, M., Troch, P. A., Mcglynn, B. L., Harman, C. J., Gupta, H. V., Kumar, P., Rao, P. S. C., Basu, N. B., and Wilson, J. S.: The future of hydrology: An evolving science for a changing world, *Water Resour. Res.*, 46, W05301, doi:10.1029/2009WR008906, 2010.
- Western, A. W., Grayson, R. B., and Bloschl, G.: Scaling of soil moisture: A hydrologic perspective, *Ann. Rev. Earth Planet. Sci.*, 30, 149–180, doi:10.1146/annurev.earth.30.091201.140434, 2002.
- Wilson, T. and Meyers, T.: Determining vegetation indices from solar and photosynthetically active radiation fluxes, *Agr. For. Meteorol.*, 144(3–4), 160–179, 2007.
- Wu, H. and Li, Z.-L.: Scale Issues in remote sensing: A review on analysis, processing and modeling, *Sensors*, 9, 1768–1793, doi:10.3390/s90301768, 2009.